Status and recent dark matter search results from the PandaX experiment

Mengjiao Xiao[1,2] *(On Behalf of PandaX Collaboration)*

[1] Department of Physics, University of Maryland, College Park, USA
[2] Institute of Nuclear and Particle Physics (INPAC), Shanghai Jiao Tong University, China

DOI: http://dx.doi.org/10.3204/DESY-PROC-2016-03/Xiao_Mengjiao

The PandaX project is a staged xenon-based deep underground experiment at the China Jin-Ping Underground Laboratory. The first phase experiment, PandaX-I, a 120 kg dark matter detector using the dual phase xenon time projection chamber (TPC) technology was completed in 2014 with a 54×80.1 kg-day exposure. Recently, the commissioning run of the second phase of the experiment, PandaX-II, was completed with a 306×19.1 kg-day exposure. We report the status of the PandaX experiment, and then present the dark matter search results from both runs.

1 Introduction

PandaX experiment is located in the China Jin-Ping Underground Laboratory (CJPL) in south-east China. The average depth is 2400 m or 6800 m w.e (water equivalent depth) where the muon flux is reduced to around 60 events/m^2/year [1]. The project is developed stagewise. In PandaX-I, the first phase of the project, 120 kg active liquid xenon was contained in the central detector to search for the Weakly Interaction Massive Particles (WIMPs). In the second phase, PandaX-II, the target mass for the WIMP detector was enlarged to a half tone. The PandaX-III, the future phase of the project, will use the high pressure ^{136}Xe gas to search for neutrinoless double beta decay. The collaboration also aim to develop a multi-ton liquid xenon detector for dark matter search. Currently we have completed PandaX-I, and PandaX-II is undergoing.

In PandaX-I and PandaX-II, the dual-phase xenon time projection chamber (TPC) technology, illustrated in Fig. 1, was adopted for WIMP dark matter detection. An incoming particle interaction in the liquid xenon (LXe) produces direct scintillation photons, called S1, as well as the ionization electrons. An electrical field is applied across the liquid xenon volume. The ionization electrons drift to the liquid-gas interface and are extracted into the gaseous xenon by a stronger electrical field, producing secondary proportional scintillation photons, which are called S2. Both signals (S1 and S2) can be detected by the photomultiplier tube (PMT) arrays located at top and bottom of the detector. The time difference of the two signals can be used to calculate the vertical position of the interaction. The S2 signal pattern in the top array allows the reconstruction of the horizontal position. Precise determination of the position of an event enables the fiducialization of a low background target region.

In Fig. 2, the discrimination power of a dual phase xenon TPC is illustrated. Compared to the electron recoil (ER) background, the ionization density of nuclear recoil (NR) signal is much

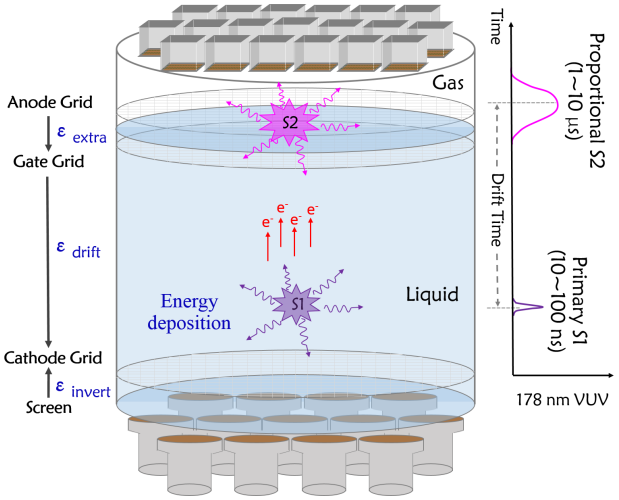

Figure 1: Work principle of a dual phase xenon TPC.

larger, so electrons are more likely to recombine with ions, leading to a relatively smaller S2-to-S1 ratio. Therefore this ratio can be used to discriminate nuclear and electron recoil events. Additionally,dark matter particles can only scatter once in the detector, so the background can be further suppressed by the requirement of single scattering.

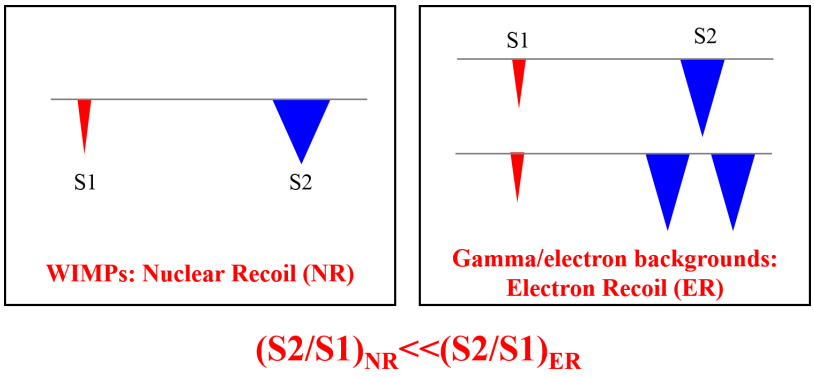

Figure 2: Bacrground discrimination with a dual phase xenon TPC.

2 PandaX-I dark matter search results

The PandaX-I setup is described in detail in Ref. [2]. Fig. 3 shows the TPC design of the PandaX-I experiment. It was a pancake structure, with a drift volume of 60 cm in diameter and 15 cm in height. We had 143 1-inch PMTs (Hamamatsu R8520-406) and 37 3-inch PMTs (Hamamatsu R11410-MOD) with quantum efficiency peaked at 178 nm on the top and bottom,

respectively. To increase the light collection efficiency, PTFE reflectors were installed around the TPC. The electrical field in the TPC was defined by three electrodes, the cathode, gate and anode. During the operation, the anode grid was grounded while separated by 8 mm with the gate grid located 4 mm below the liquid level. High voltage with -15 kV and -5 kV was applied on to the cathode and gate grids respectively. Outside the refelector wall, the shaping rings were used to regularize the drift field. The design goal of the TPC is to achieve good light collection efficiency which is a key to detect low-mass dark matter. The right pictures in Fig. 3 show the real TPC components serving for PandaX-I. From top to bottom, they are the top PMT array, field cage and the bottom PMT array.

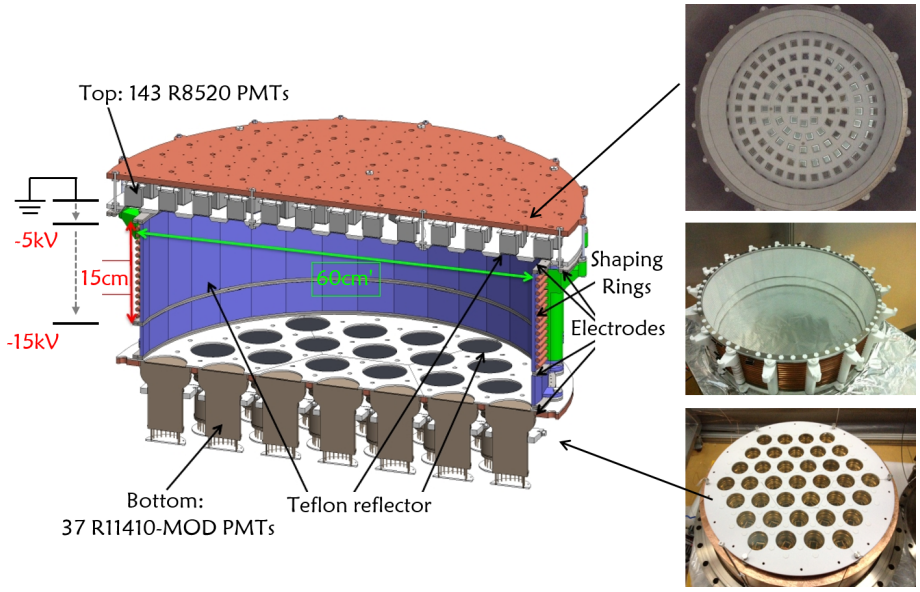

Figure 3: PandaX-I TPC design and pictures.

PandaX-I dark matter search experiment took physical data from May 26, 2014 to Oct. 16, 2014. With a blinded data analysis, we released the dark matter search results with an exposure of 80.1 day $\times$ 54 kg [14]. No positive signal above the background was found. We set the 90% C.L. exclusion limit to the dark matter interaction with nucleon, and the lowest excluded cross section is at about $1\text{x}10^{-44}$ cm^2 for a WIMP mass of 44.7 GeV/c^2. The result strongly disfavors previously reported signals from the DAMA/LIBRA [3], CoGeNT [4], CDMS-II-Si [7] and CRESST-II [5] experiments. Our result offers tighter bound above 7 GeV/c^2 than SuperCDMS. In the xenon experiment community, at that time, we achieved the best reported limit below 5.5 GeV/c^2.

3 Recent updates from the PandaX-II experiment

In parallel with the running of PandaX-I, we started to prepare the PandaX-II detector in 2014. Most of the infrastructures of PandaX-I were reused for PandaX-II: passive shielding, outer Cu vessel, cryogenics, etc. The experiment was located at the same experimental hall in CJPL.

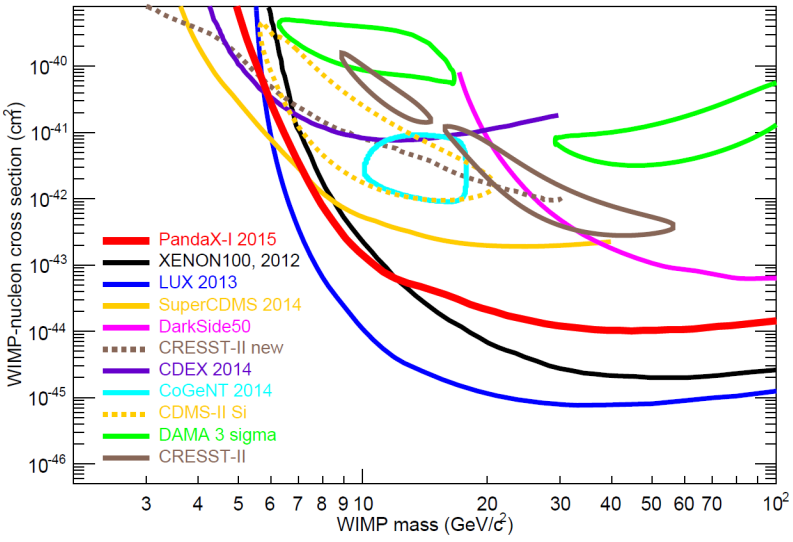

Figure 4: The 90% c.l. upper limit for spin-independent isoscalar WIMP-nucleon cross section for the PandaX-I experiment (red curves). Recent world results are plotted for comparison: XENON100 225 day results [9] (black solid), LUX first results [10] (blue), SuperCDMS results [17] (orange solid), DarkSide results [18] (magenta solid), CRESST-II 2014 limits [5] (brown dashed), and CDEX 2014 limits [6] (solid violet). The claimed WIMP signals are shown as closed contours: CoGeNT 2014 results [4] (cyan solid), CDMS-II-Si results [7] (gold dashed), DAMA/LIBRA 3σ contours [3] (green solid), and CRESST-II 2012 results [5] (brown solid).

The most significant upgrades were the new inner vessel constructed from stainless steel with much lower radioactivity, and a much larger xenon TPC. The cylindrical TPC, as shown in Fig. 5, contains 580 kg LXe in the sensitive volume with an inner diameter of 646 mm and a maximum drift length of 600 mm. In addition, we placed 55 Hamamatsu-R11410-MOD 3-inch PMTs on the top and bottom of the TPC respectively, and added 48 R8520-406 1-inch PMTs outside the target serving as active veto. To further increase the light collection efficiency, the PTFE plates with higher reflectivity were selected to enclose the TPC.

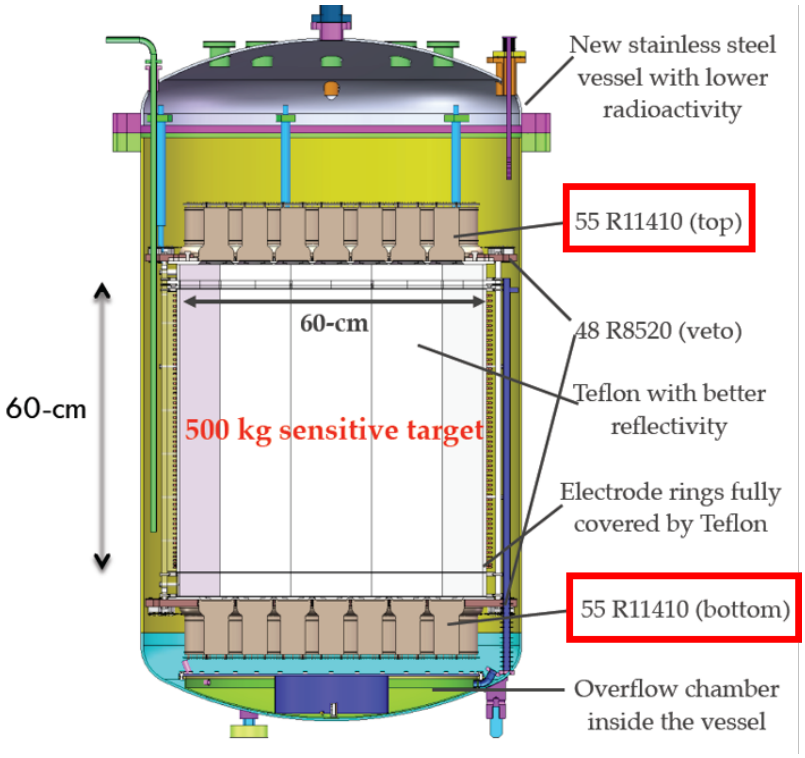

Figure 5: The TPC design of the PandaX-II experiment.

The onsite installation of detector for PandaX-II started in October of 2014. We spent around one year to take series of engineering runs in 2015 to test all the components. A physics commissioning run from Nov.22 to Dec.14 was carried out but ended due to high Krypton background [15]. Here we present the performance of the detector in PandaX-II experiment and the dark matter search results from this commissioning run.

3.1 Detector calibration

During the operation, high voltage of -29 kV and -4.95 kV was applied to the cathode and gate grid, respectively, and the anode was kept at ground. We deployed one neutron source (^{252}Cf) and two gamma sources (^{60}Co and ^{137}Cs) close to the inner detector to calibrate the detector response. Neutrons can excite xenon nuclei or produce metastable nuclear states, leading to de-exciting gamma rays at 40 (^{129}Xe), 80 (^{131}Xe), 164 (^{131m}Xe), and 236 keV (^{129m}Xe). These

energy peaks are used to study the non-uniformity of the detector and extract the detector's parameters. With liquid xenon TPC, any energy deposition in LXe will be released in the form of either S1 or S2. An electron equivalent deposited energy can be reconstructed with Eq. 1 in which $W = 13.7$ eV is the average work function to produce either an electron or photon, PDE is photon detection efficiency, SEG is single electron gain and EEE is electron extraction efficiency.

$$E_{ee} = W \times (\frac{\text{S1}}{\text{PDE}} + \frac{\text{S2}}{\text{SEG} \times \text{EEE}}) \tag{1}$$

We fitted the photonelectron distribution of the smallest S2 signals with a Gaussian function and obtained SEG = 22.1±0.7 PE/e$^-$. Through the anti-correlation between S1 and S2 for various energy peaks, other parameters in Eq. 1 were obtained with a linear fit as shown in Fig. 6. The best fit values are PDE = 11.7%, EEE = 48.1% with the uncertainty of 5.6% and 7.1% respectively.

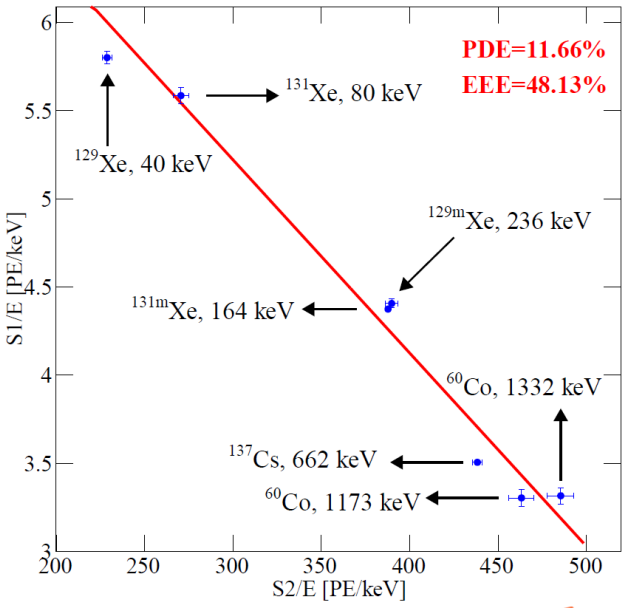

Figure 6: Linear fit in S2/E$_{ee}$ vs. S1/E$_{ee}$ for all energy peaks.

The neutron events in ^{252}Cf calibration data were used to study the detector's response to nuclear recoil signals. In the operation, we obtained 547 events in the target volume for S1 between 3 to 45 PE. The $\log_{10}$(S2/S1) vs. S1 of these events is shown in Fig. 7. Based on the NEST model [12, 13] and the PDE, EEE and SEG obtained above, we peformed a full Monte-Carlo (MC) simulation using Geant4. The MC predication is also overlaid in Fig. 7. A better agreement on the median of the NR distribution can be achieved by tuning the ratio of the initial number of excitation and ionization by a factor of 1.5 in the NEST model. The tunned MC was chosen as the default model. The NR detection efficiency was obtained by the comparison of data and MC predication, parameterized as a function both of S1 and S2 shown

in Eq. 2, where $S2_{raw}$ is the raw S2 before the electron lifetime correction.

$$\epsilon = 0.94[e^{-\frac{S1-6.21}{1.66}} + 1]^{-1}[e^{-\frac{S2_{raw}-79.3}{20.8}} + 1]^{-1} \quad (2)$$

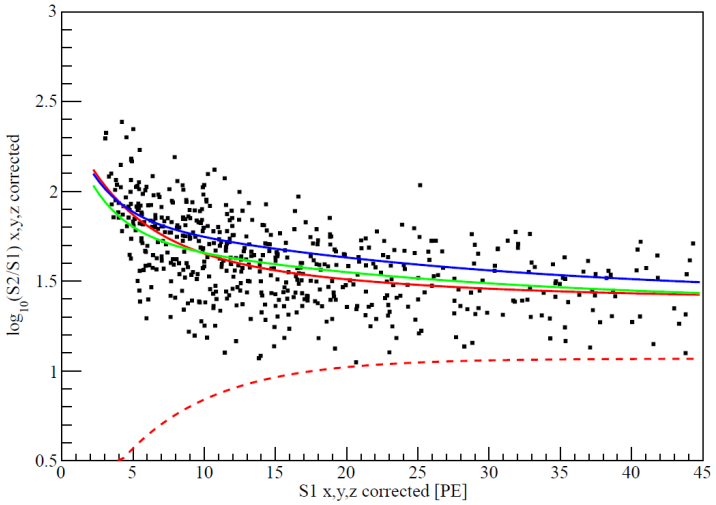

Figure 7: The comparison of ^{252}Cf neutron calibration data with the median from the original NEST model (blue line) and the tuned model (green line). A fit to the median of the data is given by the red line. The dashed red line is the NR 99.99% acceptance line based on the tuned MC model.

3.2 Backgrounds

As in Ref. [14], the background is categorized into three components: the ER, neutron, and accidental background. The ER background consists of external background due to radioactivities in the detector materials, and internal backgrounds due to krypton and radon. Before the detector assembly, the components were assayed with a high purity Germanium counting station at CJPL [16]. These results were used as the inputs of the MC simulation to calculate the external background at low energy, which was estimated to be 0.21 mDRU (1 mDRU=10^{-3} evts/keV/kg/day).

During the commissioning run, serious Kr background was found in data, likely due to an accidental air leak in a previous engineering run. With a β-γ delayed-coincident analysis, the ^{85}Kr was estimated to be 0.082 mBq/kg or 15.04 mDRU with a 3% uncertainty. Similarly, the radon level in LXe can be evaluated by identifying β-α and α-α coincidence events in data. ^{222}Rn was estimated to be 6.57 μBq/kg in the fiducial volume (FV). ^{220}Rn was estimated to be 0.54 (^{212}Bi-^{212}Po) and 0.41 μBq/kg (^{220}Rn-^{216}Po) in the FV, respectively. The ER background components are summarized in Tab. 1.

The neutron background also come from detector components. It was estimated by the MC to be 0.06 events in the final data set after all selection cuts. Same to the analysis in Ref. [14],

Item	Background (mDRU)
^{85}Kr	15.04
^{222}Rn	0.075
^{220}Rn	0.021
PMT array & bases	0.097
PTFE wall	0.021
Inner vessel	0.045
Other Inner components	0.026
Cu outer vessel	0.016
Total	15.33

Table 1: Summary of ER backgrounds from various components.

we studied single S1 and S2 events in the data. The rate of single S1-like events was determined to be 2.8±0.1 Hz within the S1 range cut. In the same data set, 28069 single S2-like events were identified within the final S2 range cut and fiducial radius cut. The accidental background was evaluated by randomly pairing the single S1 and S2 events with all coincidence selection cuts applied. 0.70 qualified accidental events were expected to survive with a 25% uncertainty.

The final expected background budget including the ER, accidental, and neutron background is summarized in Tab. 2. We expect to observe 617±104 events in the fiducal volume after the all cuts while 3.2±0.71 events are expected to below the NR median.

-	ER	Accidental	Neutron	Total Expected	Total observed
All	611	5.9	0.13	617±104	728
Below NR median	2.5	0.7	0.06	3.2±0.71	2

Table 2: The expected background events in 19.1 live-day dark matter search data in the FV, before and after the NR median cut, as well as the final number of candidate events in the data.

3.3 Dark matter search results

We searched for the dark matter signals with a total of 306×19.1 kg-day exposure. The distribution of $\log_{10}$(S2/S1) versus S1 is shown in Fig. 8(a). 728 events in total were selected for the dark matter analysis while two of these events were found below the median of the NR band. Detailed examinations confirmed the high quality of these two events. The vertex distribution of these events is shown in Fig. 8(b). Compared to the expected background, no excess dark matter signal was found. Based on the two observed events and 3.2 expected backgrounds, the final 90% C.L. upper limit for the spin-independent isoscalar WIMP-nucleon cross section was calculated using the CLs method [20, 21]. The final results are shown in Fig. 3.3. The upper limits lie in the $\pm1\sigma$ sensitivity band. The lowest cross section limit obtained is 2.97×10^{-45} cm^2 at a WIMP mass of 44.7 GeV/c^2, which represents an improvement of more than a factor of three from PandaX-I. The cross section limit at WIMP mass of 10, 100, and 300 GeV/c^2 are 8.43×10^{-44}, 4.34×10^{-45}, and 1.13×10^{-44} cm^2, respectively.

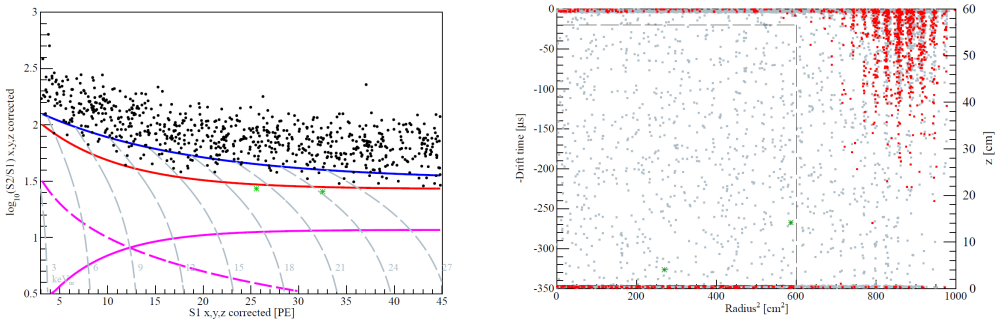

(a) (b)

Figure 8: (a) The distribution of $\log_{10}$(S2/S1) versus S1 for dark matter search data. The median of the NR calibration band is indicated as the red curve. The dashed magenta curve is the equivalent 100 PE cut on S2. The solid magenta and blue curves are the 99.99% and 33.3% NR acceptance curves, respectively. The grey dashed curves are the equal energ curves with NR energy indicated in the figures. The two data points located below the NR median curve are highlighted in green stars. (b) Position distribution of events that pass all selection cuts (gray points), and those below the NR median (outside FV: red points; inside FV: green stars), with FV cuts indicated as the black dashed box.

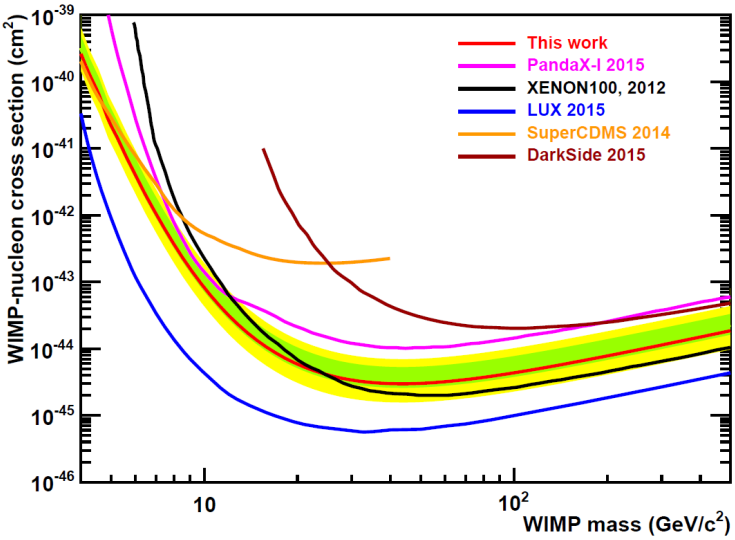

Figure 9: The 90% C.L. upper limit for the spin-independent isoscalar WIMP-nucleon cross section from the PandaX-II commissioning run (red). A selected set of recent world results are plotted for comparison: PandaX-I final results [14] (magenta), XENON100 225 day results [9] (black), LUX 2015 results [11] (blue), SuperCDMS [17] (orange), and Dark-Side 2015 [19] results (brown). The 1σ and 2σ sensitivity bands are shown in green and yellow, respectively.

4 Conclusion and outlook

The PandaX experiment has been producing tight constrains to the WIMP parameter space. The half-ton scale DM experiment of PandaX-II has been commissioned with key components working. No dark matter signal was observed in the commissioning run with an exposure of 306×19.1 kg-day. After the commissioning run, we carried out a distillatation to remove Kr, afterward the ER background was suppressed significantly. The physics data taking was resumed this year. After this conference, PandaX-II released the dark matter results with a total exposure of 3.3×104 kg day [22] and set the world's best reported limit on the spin-independent elastic WIMP-nucleon cross sections.

References

[1] Wu Y C, Hao X Q, Yue Q, *et al.*, "Measurement of cosmic ray flux in China JinPing underground Laboratory", Chin Phys C, 2013, 37 (8): 086001.

[2] Cao X G, Chen X, Chen Y H, *et al.* [PandaX Collaboration]. "PandaX: A liquid xenon dark matter experiment at CJPL", Sci China-Phys Mech Astron, 2014, 57(8): 14761494.

[3] R. Bernabei *et al.* [DAMA Collaboration], Eur. Phys. J. C 56 (2008), Eur. Phys. J. C 67 (2010), Eur. Phys. J. C 73 (2013).

[4] C. E. Aalseth *et al.* [CoGeNT Collaboration], Phys. Rev. Lett. 106, 131301 (2011), Phys. Rev. D88, 012002 (2013), and latest analysis using maximum likelihood method in arXiv:1401.6234 (2014)

[5] G. Angloher et al. [CRESST Collaboration], Eur. Phys. J. C 72 (2012), Eur. Phys. J. C 74 12, 3184 (2014)

[6] Q. Yue *et al.* [CDEX Collaboration], "Limits on light weakly interacting massive particles from the CDEX-1 experiment with a p-type point-contact germanium detector at the China Jinping Underground Laboratory", Phys. Rev. D 90, 091701 (2014)

[7] R. Agnese *et al.* [CDMS Collaboration], "Silicon Detector Dark Matter Results from the Final Exposure of CDMS II", Phys. Rev. Lett. 111, 251301 (2013)

[8] M. Xiao *et al.* [PandaX Collaboration], "First dark matter results from the PandaX-I Experiment", Sci. China Phys. Mech. Astron. 57, 2024 (2014) [arXiv:1408.5114 [hep-ex]].

[9] E. Aprile *et al.* [XENON100 Collaboration], "Dark Matter Results from 225 Live Days of XENON100 Data", Phys. Rev. Lett. 109, 181301 (2012), [arXiv:1207.5988 [astro-ph.CO]].

[10] D. S. Akerib *et al.* [LUX Collaboration], "First Results from the LUX Dark Matter Experiment at the Sanford Underground Research Facility", Phys. Rev. Lett. 112, 091303 (2014), [arXiv:1310.8214 [astro-ph.CO]].

[11] D. S. Akerib *et al.* [LUX Collaboration], "Improved Limits on Scattering of Weakly Interacting Massive Particles from Reanalysis of 2013 LUX Data", Phys. Rev. Lett. 116, 161301 (2016), [arXiv:1512.03506 [astro-ph.CO]].

[12] M. Szydagis, N. Barry, K. Kazkaz, J. Mock, D. Stolp, M. Sweany, M. Tripathi, S. Uvarov, N.Walsh, and M Woods, "NEST: A Comprehensive Model for Scintillation Yield in Liquid Xenon", J. Instrum. 6, P10002 (2011),]arXiv:1106.1613v1 [physics.ins-det]].

[13] M. Szydagis, A. Fyhrie, D. Thorngren, and M. Tripathi, "Enhancement of NEST Capabilities for Simulating Low-Energy Recoils in Liquid Xenon", J. Instrum. 8, C10003 (2013), [arXiv:1307.6601v1 [physics.ins-det]].

[14] X. Xiao *et al.* [PandaX Collaboration], "Low-mass dark matter search results from full exposure of PandaX-I experiment", Phys. Rev. D92, 052004 (2015) [arXiv:1505.00771 [hep-ex]].

[15] A. Tan *et al* [PandaX Collaboration], "Dark Matter Search Results from the Commissioning Run of PandaX-II", Phys. Rev. D93, 122009 (2016) [arXiv:1602.06563 [hep-ex]].

[16] Xuming Wang, Xun Chen, Changbo Fu, Xiangdong Ji, Xiang Liu, Yajun Mao, Hongwei Wang, Siguang Wang, Pengwei Xie, Tao Zhang "Material Screening with HPGe Counting Station for PandaX Experiment", [arXiv:1608.08345 [physics.ins-det]]

[17] R. Agnese *et al.* [SuperCDMS Collaboration], "Search for Low-Mass Weakly Interacting Massive Particles with SuperCDMS", Phys. Rev. Lett. 112, 241302 (2014), [arXiv:1402.7137 [hep-ex]].

[18] P. Agnes *et al.* [DarkSide Collaboration], "Low radioactivity argon dark matter search results from the DarkSide-50 experiment", Phys. Lett. B743, 456 (2015), [arXiv:1510.00702v2 [astro-ph.CO]].

[19] P. Agnes *et al.* [DarkSide Collaboration], "Results from the first use of low radioactivity argon in a dark matter search", Phys. Rev. D 93, 081101 (2016), [arXiv:1510.00702 [astro-ph.CO]].

[20] A. L. Read, "Presentation of search results: the CL_s technique", J. Phys. G28, 2693 (2002).

[21] T. Junk, Nucl. Instrum. Meth. A434, 435 (1999), [arXiv:9902006 [hep-ex]].

[22] A. Tan *et al.* [PandaX-II Collaboration], "Dark Matter Results from First 98.7 Days of Data from the PandaX-II Experiment", Phys. Rev. Lett. 117, 121303 (2016), [arXiv:1607.07400 [hep-ex]].